RSC Advances

PAPER

Cite this: *RSC Adv.*, 2023, **13**, 22172

Solubility determination, dissolution properties and solid transformation of resmetirom (form A) in heptane and seven alcohols†

Chang Liu,‡ Yue Xu,‡ Haikuan Yuan,* Guangxin Tian, Xiaolan Qin, Boxuan Lou, Xijian Liu, Lijuan Zhang and Jie Lu*

In this work, the solubility of resmetirom (form A) was initially measured in heptane and seven alcohol solvents by gravimetric methods. Then, the transformation temperature between form A and ethanol solvate was determined at 333.76 K. Subsequently, some commonly used models were applied to fit the solubility data, and it was found that the modified Apelblat equation and the Jouyban–Acree–van't Hoff (J–A–V) model achieved the highest correlation accuracy for those in mono-solvents and heptane + propanol, respectively. And the average relative deviation (ARD) values of models were less than 0.5%, indicating a good agreement with the experimental results. Additionally, through density functional theory calculation and the analysis of solvent parameters, it was observed that hydrogen-bonding played primary roles in the dissolution process of resmetirom. The multiple factors such as the polarity of solvent, active site interaction, the molecular size and free volume all affect the solubility of resmetirom. Furthermore, by comparing the experimental and simulated infrared spectra of form A and two alcohol solvates, five characteristic bands were selected for quantification. Partial least squares regression (PLSR), a multivariate statistical analysis method, was used to extract quantitative information. The quantitative analysis model was established based on specific wavelength intervals, which were associated with intermolecular interactions. Combined with PLSR, a new high-precision quantitative method was established to study the solid transformation process between form A and solvates. From 303.15 to 323.15 K, the rate of transformation from form A to methanol solvate or ethanol solvate was decreased with increasing temperature, revealing that the transformation process was driven by the solubility difference between form A and solvates under the studied conditions. This research will definitely afford necessary solubility data and solvent selection for the design of the crystallization process of resmetirom (form A) in industry, and provide basic data for the production of resmetirom (form A) in the pharmaceutical industry.

Received 16th April 2023
Accepted 17th July 2023

DOI: 10.1039/d3ra02521g

rsc.li/rsc-advances

Introduction

Active pharmaceutical ingredients (APIs) have been proven to commonly possess various solid forms, in which more than half of the APIs are able to form solvates.[1,2] Because of different conformations and arrangements of active molecules as well as disparate binding types of solvent molecules in solid structures, different solid forms of drug molecules often show various physicochemical properties, processing performance, solubility and bioavailability, leading further to different therapeutic effect and safety. Hence, research on the different solid forms of APIs is crucial in the drug development process.[3–5]

Various solvents are inevitably used in drug production, and the transformation of certain crystalline forms turning to solvates are common.[6] Therefore, the study of solid transformation is vital for drug production. The solid–solid transformation kinetics model is typically obtained through online or offline detection techniques such as differential scanning calorimetry (DSC), powder X-ray diffraction (PXRD), Fourier transform infrared (FTIR), *etc.*[7,8] Among them, FTIR is an ideal method for the quantitative analysis to study the conversion between different solid forms because of its easy operation, high sensitivity and rich spectral information. The vibrational frequency of the molecule is characterized by the atomic structure, in which functional groups can be easily detected on spectra with the wavenumber from 4000 to 400 cm^{-1} and 3600 spectral points (*i.e.*, variables) were produced. However, low root mean square errors in prediction have been pursued blindly in current selection methods for infrared spectra, which lacks the interpretability of variables. Thereby, when requirements of quantitative analysis accuracy are satisfied,

College of Chemistry and Chemical Engineering, Shanghai University of Engineering Science, Shanghai 201620, China. E-mail: yhk12345@163.com; lujie@sues.edu.cn; Fax: +86 21 67791214

† Electronic supplementary information (ESI) available: Parameters of models. See DOI: https://doi.org/10.1039/d3ra02521g

‡ These authors contributed equally to this work.

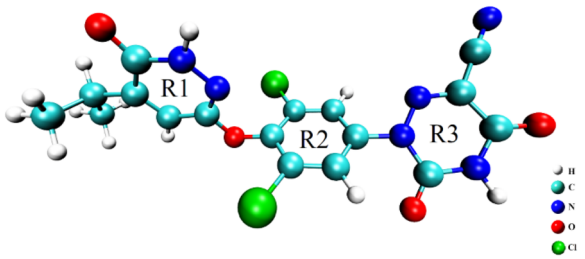

Fig. 1 Molecular structure of resmetirom.

improvement on interpretability of variable selection is one of the development directions of variable selection methods.[9,10]

The concept of "nonalcoholic steatohepatitis (NASH)" was first introduced by Ludwig in 1980,[11] and in 1986, Schaffner introduced "nonalcoholic steatohepatic disease (NAFLD)".[12] NASH is considered the most severe histological lesion within NAFLD due to its higher propensity for hepatocellular carcinoma development. NASH patients exhibit a fibrosis progression rate of 40.76% and a mean annual progression rate.[13] Recent estimates suggest that NASH will lead to a 30% increase in indirect and direct healthcare costs over the next 5 years due to rising rates of overweight and obesity. Consequently, the development of therapeutic drugs for NASH is urgently needed. Resmetirom is a highly selective THR-β agonist with the ability to regulate lipid metabolism, and Phase III clinical trials of its therapy for NASH have been finished.[14,15] The molecular structure of resmetirom is depicted in Fig. 1, which includes pyridazine ring (R1), dichlorobenzene ring (R2) and triazine ring (R3) from left to right. The Hansen solubility parameters of resmetirom in variously chosen solvents and the single-crystal structure of the solvates were acquired by Tian *et al.*[16] However, solubility and solid transformation in organic solvents remains unreported.

Building upon the work of Tian *et al.*,[16] the solubility of resmetirom (form A) in heptane and seven alcohol solvents was firstly determined in this study, which were correlated using four commonly used models. Then, the dissolution process of resmetirom could be analyzed based on the binding energy calculation by density functional theory (DFT). Subsequently, combined with DFT calculations, a vibrational frequency range was chosen, which was sensitive to the frequency change caused by solvent molecules in the lattice.[17,18] Finally, based on variable selection method, a high-precision quantitative analysis was built up by partial least squares regression (PLSR), which was adopted to reveal the impact on temperatures to transformation processes between form A and two solvates.

Materials and method

Materials

The resmetirom (form A), methanol, ethanol, propanol, isopropyl alcohol, butanol, isobutyl alcohol, 3-methyl-1-butanol and heptane were supplied by Aladdin Company (Shanghai, China). Details of these materials were given in Table 1.

Characterization

The solid-state characterization methods used in this work included DSC, PXRD and FTIR. Based on the principle of power-compensated heat flow differences, the DSC data were obtained by an STA 499 F1 differential scanning calorimeter (Netzsch, Bavaria, Germany) armed with a mainframe, a workstation and a gas controller. The PXRD spectrum were obtained by a multifunctional Fringe EV X-ray diffractometer (LANScientific, Jiangsu, China), Cu-Kα radiation ($\lambda = 1.54$ Å) with a tube voltage of 40 kV and a tube current of 35 mA was used to analyze samples over 2θ range of 5–45°, and imaged by MDI Jade 6.5 software. The FTIR data were collected on a Shimadzu IRTracer-100 spectrometer (Shimadzu, Tokyo, Japan) and imaged on Omnic software.

Solubility measurement

From 273.15 to 333.15 K, the solubility of form A was determined in seven mono-solvents as well as mixed solvent of heptane + propanol using a gravimetric method. Firstly, the appropriate organic solvent was added to a crystallizer, and excess samples were added at desired temperatures. Then, the commixture was stirred utilizing magnetic stirrers for 12 h, and stood for another 12 h until the suspension reached solid–liquid equilibrium. Subsequently, the supernatants were withdrawn using preheated syringes, followed by being transferred to a pre-weighed sample vial. After that the filtrate and vial were weighted by an FA1004T analytical balance (Supo, Zhejiang, China), followed by being dried in a constant-temperature

Table 1 Detailed information of materials used in this work

Material	Molecular formula	Molar volume ($cm^3\ mol^{-1}$)	Molar mass ($g\ mol^{-1}$)	Mass fraction purity	Analytical method
Resmetirom	$C_{17}H_{13}Cl_2N_5O_6$	263.77	435.22	≥0.990	HPLC[a]
Methanol	CH_4O	42.50	32.00	≥0.995	GC[b]
Ethanol	C_2H_5O	58.39	46.07	≥0.995	
Propanol	C_3H_8O	75.50	60.10	≥0.995	
Isopropyl alcohol	C_3H_8O	75.90	60.10	≥0.995	
Butanol	$C_4H_{10}O$	92.00	74.12	≥0.995	
Isobutyl alcohol	$C_4H_{10}O$	92.40	74.12	≥0.995	
3-Methyl-1-butanol	$C_5H_{12}O$	108.90	88.15	≥0.995	
Heptane	C_7H_{16}	144.00	100.20	≥0.995	

[a] High performance liquid chromatography [b] Gas chromatographic method.

WGL-65B oven (Taisite, Tianjin, China) until the mass kept unchanged. Finally, the crystalline forms of residual solids were characterized. The reported experimental data were averaged of three experiments. The molar fraction solubility of form A (x_i) in mono-solvent and binary solvent system were calculated using eqn (1):[19–21]

$$x_i = \frac{m_1/M_1}{m_1/M_1 + \omega m_2/M_2 + (1-\omega)m_2/M_3} \quad (1)$$

where M_1, M_2, M_3 were the molecular mass of form A, alcohols as well as heptane, respectively. m_1 and m_2 were the mass of form A and solvent, respectively. ω was the mass fraction of propanol in mixed solvents.

Solid transformation determination

The solid transformation experiments for form A were carried out in 50 mL crystallizer. Firstly, in light of solubility data above, initial suspend solutions of form A at 303.15, 313.15, and 323.15 K were prepared in 10 g methanol/ethanol. Then the suspension was extracted and filtered in an interval time, and residual solids were dried at corresponding temperature for 30 min. Finally, a high-precision calibration of FTIR for quantitative analysis was used in this study, and the purity of the methanol solvate (R-MT) and ethanol solvate (R-ET) was determined.

Establishment of quantitative analysis methods

Firstly, form A and the two solvates were weighed accurately. Then, characterization of the solids was detected on PXRD to confirm that no polymorphic transition occurred during the measurements. After that, fifteen samples were prepared in the 0–100% concentration range, and all of which were mixed in 5 mL vials followed by being shaken for 15 min. Subsequently, the small samples were further ground with 200 mg KBr powder. The powder was mixed thoroughly in an agate mortar and tableted into transparent discs with a diameter in approximately 1 cm by an FW-5A tablet press machine (Shengda, Tianjin, China). Multiple measurements on the samples to decrease the error of quantitative analysis. Finally, the full processes of quantitative analysis were completed of the PLSR method on Matlab 2020 software.[22,23]

All quantum calculations were used in the Gaussian16 software with the B3LYP exchange–correlation functionals and the 6-311G (d, p) basis set, combined with the BJ-damping function proposed by Grimme to account for long-range effects.[24] In order to establish a more precise quantitative analysis model, geometry optimization and vibrational analysis were carried out for both form A and solvates, meanwhile, FTIR spectra were simulated. The correction factor (0.961) was also applied to calibrate all calculated vibrational frequencies. The simulated FTIR spectra showed no imaginary frequencies, indicating that the optimized molecule corresponded to the minimum of the potential energy surface. For improvement of model performance, PLSR, a multivariate statistical analysis method, was used to extract quantitative information to overcome the nonlinear relationship between spectral response signals and concentrations. The quantitative analysis model was established based on specific wavelength intervals, which were associated with inter-molecular interactions. The coefficient of determination, R^2, which was worked as an indicator of assessing model accuracy, was calculated as follows:

$$R^2 = 1 - \frac{\sum_{i=1}^{n}(y_i - y_P)^2}{\sum_{i=1}^{n}(y_i - y_m)^2} \quad (2)$$

here, n represented the sample size. y_P, y_i and y_m were denoted as the predicted, actual and mean values of the sample, respectively.

Quantum mechanics calculation

The simulations pertaining to resmetirom molecules were performed using DFT in the Gaussian16 software. Firstly, the structures of resmetirom molecules and various solvent molecules were optimized and verified by frequency calculations, ensuring that the potential energy surface on their structures was a local minimum. Then, the optimized molecular structures were plotted separately for the electrostatic distribution on the molecular surface. Based on the principle of potential attraction, the possible interaction sites of solvent–solute molecules were predicted. Subsequently, the solvent and solute molecules were placed at suitable positions as the initial conformation according to the predicted sites, and the optimization of structure, position, and frequency calculation were performed again. The optimized solute–solvent units were analyzed by interaction region indicator (IRI) to calculate the intermolecular interaction forces. The Multiwfn software calculated the molecular electrostatic potential (MEP) maps and IRI analysis maps, which were presented in the VMD 1.9.4 program.[25,26] Finally, binding energies (ΔE) corrected by basis set superposition error (BSSE) between resmetirom and various solvents was calculated using DFT to quantify the binding abilities of the solute with different solvents at the B3LYP-D3 (BJ)/6-311G (d,p) level. ΔE was expressed as:[27–29]

$$\Delta E = E_{unit} - (E_A + E_B) + E_{BSSE} \quad (3)$$

here, E_{unit}, E_A, E_B and E_{BSSE} represented the energy of solute–solvent unit, solute molecules, solvent molecules and BSSE, respectively.

Results and discussion

Characterization

The solids are dried for 30 min to remove surface solvent, and they are subsequently performed using PXRD. The PXRD patterns of the solid residues and resmetirom (form A) are depicted in Fig. 2. When methanol and ethanol are solvents, the PXRD patterns of residual solids are different to form A, indicating that two solvates are formed. The peaks of residual solids in other solvents are basically similar except in methanol and ethanol, indicating that solvates are not formed. The characteristic peaks of form A are identified at $2\theta = 8.19 \pm 0.1°$, $11.16 \pm 0.1°$, $18.32 \pm 0.1°$, $18.67 \pm 0.1°$, $22.23 \pm 0.1°$ and $32.20 \pm 0.1°$. The characteristic peaks for R-MT appear at $2\theta = 5.71 \pm 0.1°$,

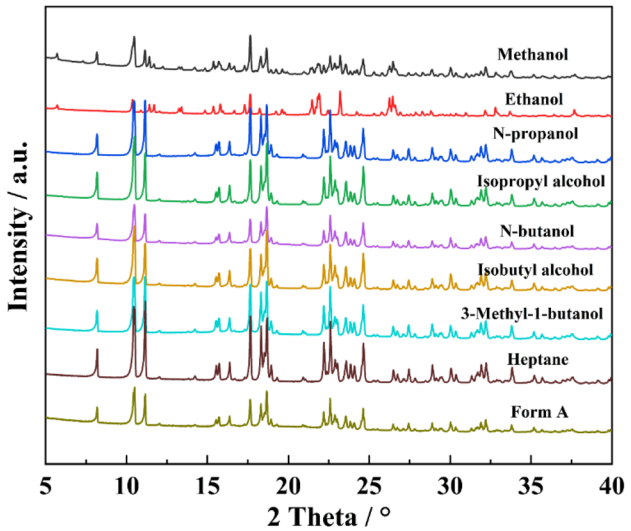

Fig. 2 PXRD diagrams of form A as well as residual solids for solubility measurements.

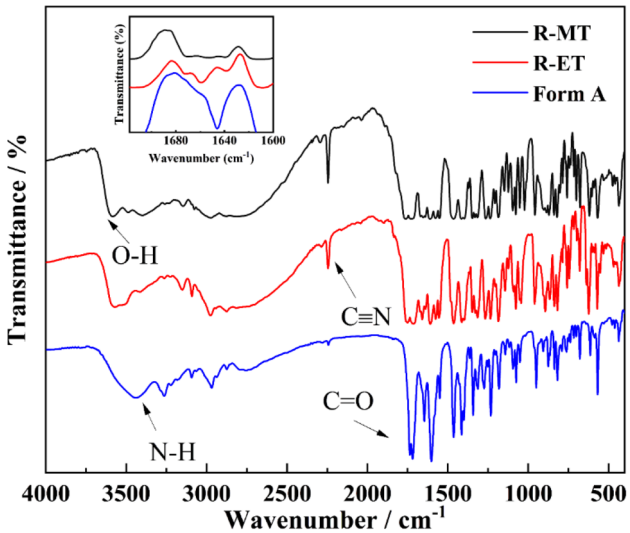

Fig. 4 FTIR spectra of form A, R-MT and R-ET. The embedded figure is a schematic diagram of some bands.

10.46 ± 0.1°, 17.65 ± 0.1°, 22.59 ± 0.1°, 24.61 ± 0.1°. The characteristic peaks for R-ET appear at $2\theta = 5.71 \pm 0.1°$, 10.52 ± 0.1°, 11.41 ± 0.1°, 21.19 ± 0.1°, 23.19 ± 0.1°, 26.24 ± 0.1°.

Form A, R-MT, and R-ET forms of DSC and TGA curves are illustrated in Fig. 3(a)–(c), respectively. At 606.30 K, the crystals start to decompose and melt with an enthalpy of decomposition of 120.32 J g^{-1}. The DSC curves of the solvates show a clear endothermic peak before the decomposition temperature. The heat absorption enthalpy of the methanol solvate is 95.97 J g^{-1}, while that of the ethanol solvate is 113.31 J g^{-1}. This is a consequence of solvent molecules evaporating from the lattice during heating. By the mass loss on TGA curves, the stoichiometric ratio between the solute and solvent molecules can be obtained for two solvates, which are both 1. The theoretical and observed mass loss rates for the R-MT are 6.45% and 6.56%, respectively, while those for the R-ET are 9.57% and 9.51%, indicating the data of experimental mass loss exhibit a satisfactory agreement with the theoretical data.

The original FTIR spectra of form A, R-MT and R-ET are shown in Fig. 4, which reveal molecular vibration information is related to the crystal structure. The main difference between form A and the two solvates is reflected in the range of the 3600–3000 cm^{-1}, which is obviously due to the O–H stretching vibrations in hydroxyl and N–H stretching vibrations in amide groups. Additionally, the intensity of the C≡N peak also varies significantly, which is attributed to the intramolecular hydrogen bonding between resmetirom and the solvent molecules. The characteristic peaks in the range of 1800–1700 cm^{-1} could be ascribed to the stretching vibration of carbonyl groups. The carbonyl stretching vibrational peaks on the R3 and R1 rings in form A appear at 1736 and 1719 cm^{-1}, respectively, while the corresponding vibrations for the solvates appear at 1760 and 1727 cm^{-1}. In the range of 1700–1600 cm^{-1}, a single peak occurs in the spectrum of form A, while three small peaks occur in that of solvates (as shown in the embedded figure), which may be related to the solvent molecules in the lattice. The FTIR spectra of the two solvates are very similar, but there is a bathochromic shift in the peaks in the spectrum of R-MT compared to that of R-ET, probably due to hydrogen bonding. The main distinction of peaks between R-MT and R-ET occurs within the spectral interval of 820–700 cm^{-1}, where the O–H vibrations in hydroxyl group in the solvent molecule is caused by a N atom in the R3 ring. The spectra of solvates exhibit the difference with that of form A resulting from intermolecular interactions, which lays a foundation for quantification by FTIR spectra.

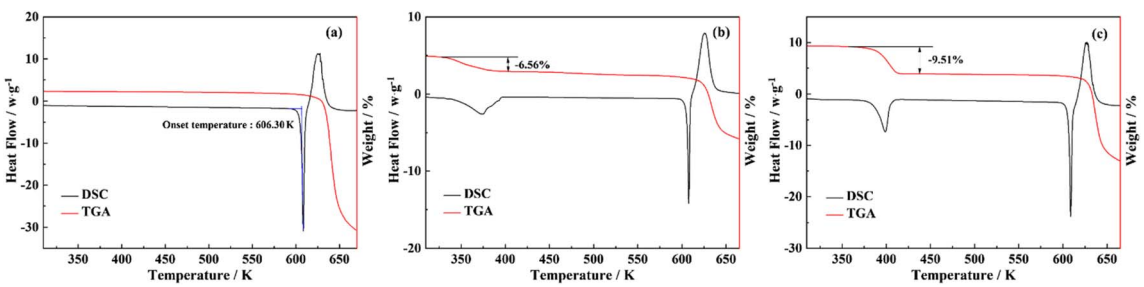

Fig. 3 DSC/TGA curves of form A (a), R-MT (b) and R-ET (c).

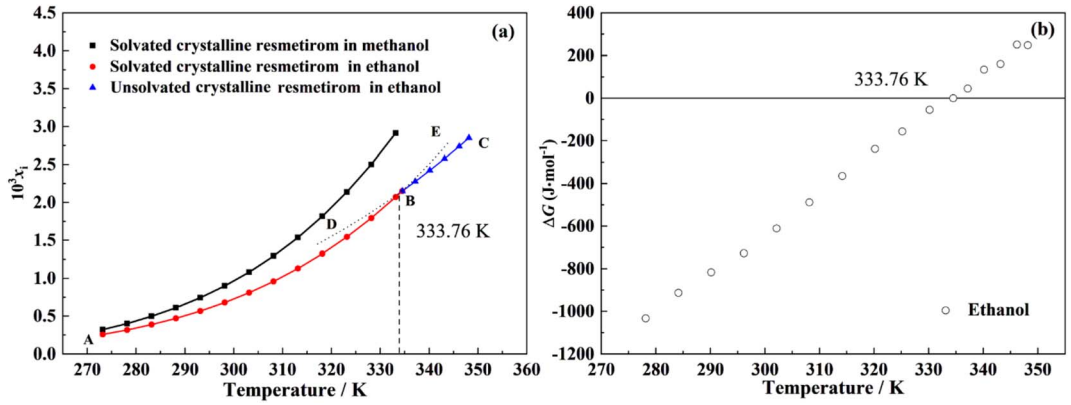

Fig. 5 Solubility of unsolvated and solvated resmetirom in methanol and ethanol (a); ΔG between form A and R-ET (b).

Table 2 Molar fraction solubility (x_i/mol mol^{-1}) of resmetirom (form A) in mono-solvents[a] (p = 0.1 MPa)

	Propanol				Isopropyl alcohol				Butanol			
		10^3x^{cal}				10^3x^{cal}				10^3x^{cal}		
T (K)	10^3x^{exp}	Apelblat	λh	Wilson	10^3x^{exp}	Apelblat	λh	Wilson	10^3x^{exp}	Apelblat	λh	Wilson
273.15	0.227	0.226	0.227	0.224	0.226	0.225	0.226	0.218	0.183	0.183	0.184	0.171
278.15	0.278	0.278	0.279	0.276	0.271	0.270	0.272	0.265	0.216	0.217	0.217	0.207
283.15	0.340	0.339	0.339	0.338	0.324	0.323	0.325	0.319	0.255	0.255	0.255	0.247
288.15	0.411	0.410	0.410	0.410	0.385	0.385	0.385	0.381	0.298	0.298	0.298	0.292
293.15	0.494	0.493	0.493	0.493	0.455	0.454	0.455	0.453	0.347	0.347	0.346	0.343
298.15	0.591	0.590	0.589	0.590	0.535	0.534	0.534	0.534	0.401	0.402	0.401	0.399
303.15	0.702	0.701	0.700	0.702	0.625	0.624	0.624	0.625	0.463	0.463	0.461	0.462
308.15	0.829	0.828	0.827	0.830	0.727	0.726	0.725	0.728	0.531	0.531	0.529	0.532
313.15	0.975	0.974	0.972	0.976	0.841	0.840	0.839	0.844	0.606	0.607	0.604	0.609
318.15	1.140	1.139	1.137	1.142	0.969	0.968	0.967	0.973	0.689	0.690	0.687	0.694
323.15	1.327	1.325	1.323	1.329	1.112	1.110	1.110	1.117	0.781	0.781	0.779	0.787
328.15	1.537	1.535	1.534	1.540	1.270	1.268	1.269	1.276	0.881	0.882	0.880	0.889
333.15	1.773	1.772	1.770	1.776	1.445	1.443	1.445	1.452	0.991	0.992	0.991	1.000
	Isobutyl alcohol				3-Methyl-1-butanol				Heptane			
		10^3x^{cal}				10^3x^{cal}				10^3x^{cal}		
T (K)	10^3x^{exp}	Apelblat	λh	Wilson	10^3x^{exp}	Apelblat	λh	Wilson	10^3x^{exp}	Apelblat	λh	Wilson
273.15	0.160	0.160	0.162	0.149	0.131	0.131	0.132	0.119	0.075	0.075	0.076	0.062
278.15	0.186	0.186	0.187	0.176	0.151	0.151	0.152	0.141	0.086	0.086	0.087	0.075
283.15	0.214	0.215	0.215	0.206	0.173	0.173	0.174	0.165	0.098	0.098	0.099	0.089
288.15	0.246	0.246	0.246	0.240	0.198	0.198	0.197	0.191	0.112	0.112	0.112	0.105
293.15	0.281	0.281	0.280	0.277	0.225	0.225	0.224	0.220	0.126	0.127	0.126	0.121
298.15	0.319	0.320	0.318	0.317	0.254	0.254	0.253	0.251	0.142	0.143	0.142	0.139
303.15	0.361	0.362	0.360	0.361	0.286	0.287	0.285	0.285	0.159	0.160	0.159	0.159
308.15	0.408	0.409	0.406	0.409	0.321	0.322	0.319	0.322	0.179	0.179	0.178	0.180
313.15	0.458	0.459	0.456	0.461	0.359	0.359	0.357	0.362	0.199	0.200	0.198	0.202
318.15	0.512	0.514	0.511	0.517	0.399	0.400	0.398	0.404	0.221	0.222	0.221	0.226
323.15	0.572	0.573	0.570	0.578	0.444	0.444	0.442	0.450	0.245	0.245	0.244	0.251
328.15	0.635	0.636	0.635	0.643	0.491	0.492	0.490	0.499	0.270	0.271	0.270	0.279
333.15	0.704	0.705	0.705	0.714	0.542	0.542	0.542	0.552	0.297	0.298	0.298	0.308

[a] The standard uncertainties u of pressure and temperature are 0.5 kPa and 0.01 K, respectively. The relative standard uncertainty of the solubility measurement is $u_r(x_i) = 0.06$.

Solubility

The stability analysis of polymorph is an essential part of pharmaceutical research. The transformation temperatures between form A and R-MT or R-ET are illustrated in Fig. 5(a). The solubility of resmetirom in ethanol vary with temperature in two temperature regions, in which the breakpoint is 333.76 K. While transformation temperature between form A and R-MT is above the boiling temperature of methanol under experimental conditions. In both temperature regions, the correlation of temperature to solubility is linear in two temperature regions, in which the slope of AB curve in low-temperature region is steeper than that of BC curve in high-temperature region. The intersection temperature point B of the two curves corresponds to 333.76 K, which is the solid transformation temperature of solvated and unsolvated forms. The solubility of the unsolvated form in the low temperature range and the solvate in the high temperature range are indicated by the two dashed lines BD and BE in the figure, respectively. According to the stability rule of crystal polymorphs, the crystal form with lower solubility has thermodynamic stability at the same temperature.[30] Therefore, when the temperature is lower than 333.76 K, the solvated crystalline form of resmetirom is stable, otherwise the form A is stable. The trend of polymorphic transformation can be explained by the difference in two forms of Gibbs free energy ΔG as follows:[31,32]

$$\Delta G = -RT\ln(x_i/x_{\text{R-ET}}) \quad (4)$$

where x_i and $x_{\text{R-ET}}$ are the solubilities of form A and R-ET at corresponding temperature, respectively. The relationship between ΔG and temperature for two forms in ethanol from 273.15 to 348.15 K is depicted in Fig. 5(b). The data from eqn (4) reveal temperature exhibits a linear relationship with ΔG. Furthermore, with a transformation point at 333.76 K, ΔG is negative at lower temperatures and positive at higher temperatures, which is congruent with the results obtained in Fig. 5(a).

Table 3 Molar fraction solubility (x_i/mol mol^{-1}) of resmetirom (form A) in propanol + heptane[a] (p = 0.1 MPa)

	$\omega = 0.2$				$\omega = 0.4$			
		10^3x^{cal}				10^3x^{cal}		
T (K)	10^3x^{exp}	Apelblat	λh	J–A–V	10^3x^{exp}	Apelblat	λh	J–A–V
273.15	0.094	0.095	0.094	0.097	0.117	0.116	0.117	0.116
278.15	0.109	0.108	0.109	0.109	0.138	0.137	0.137	0.137
283.15	0.126	0.125	0.126	0.125	0.162	0.163	0.160	0.163
288.15	0.145	0.144	0.145	0.144	0.189	0.191	0.187	0.191
293.15	0.166	0.165	0.166	0.164	0.219	0.220	0.216	0.220
298.15	0.190	0.193	0.189	0.192	0.252	0.250	0.249	0.251
303.15	0.215	0.215	0.214	0.214	0.290	0.292	0.286	0.291
308.15	0.243	0.242	0.242	0.241	0.331	0.330	0.327	0.330
313.15	0.274	0.274	0.273	0.273	0.377	0.375	0.373	0.377
318.15	0.308	0.310	0.307	0.309	0.428	0.429	0.423	0.429
323.15	0.344	0.344	0.343	0.344	0.483	0.484	0.478	0.483
328.15	0.383	0.382	0.383	0.382	0.543	0.543	0.538	0.543
333.15	0.426	0.426	0.426	0.427	0.609	0.608	0.605	0.609
	$\omega = 0.6$				$\omega = 0.8$			
		10^3x^{cal}				10^3x^{cal}		
T (K)	10^3x^{exp}	Apelblat	λh	J–A–V	10^3x^{exp}	Apelblat	λh	J–A–V
273.15	0.146	0.145	0.148	0.145	0.182	0.183	0.184	0.181
278.15	0.175	0.177	0.176	0.177	0.221	0.223	0.222	0.223
283.15	0.207	0.205	0.209	0.205	0.266	0.264	0.267	0.268
288.15	0.245	0.246	0.246	0.246	0.317	0.317	0.319	0.316
293.15	0.287	0.286	0.288	0.286	0.377	0.379	0.378	0.377
298.15	0.335	0.334	0.336	0.334	0.445	0.449	0.446	0.444
303.15	0.390	0.391	0.390	0.391	0.523	0.522	0.524	0.523
308.15	0.450	0.449	0.451	0.449	0.612	0.613	0.612	0.613
313.15	0.518	0.518	0.519	0.518	0.711	0.712	0.712	0.711
318.15	0.594	0.595	0.594	0.595	0.823	0.827	0.824	0.823
323.15	0.677	0.678	0.678	0.677	0.948	0.951	0.950	0.948
328.15	0.769	0.770	0.771	0.769	1.088	1.083	1.090	1.088
333.15	0.871	0.873	0.874	0.872	1.243	1.246	1.247	1.243

[a] The standard uncertainties u of pressure and temperature are 0.5 kPa and 0.01 K, respectively. The relative standard uncertainty of the solubility measurement is $u_r(x_i) = 0.06$.

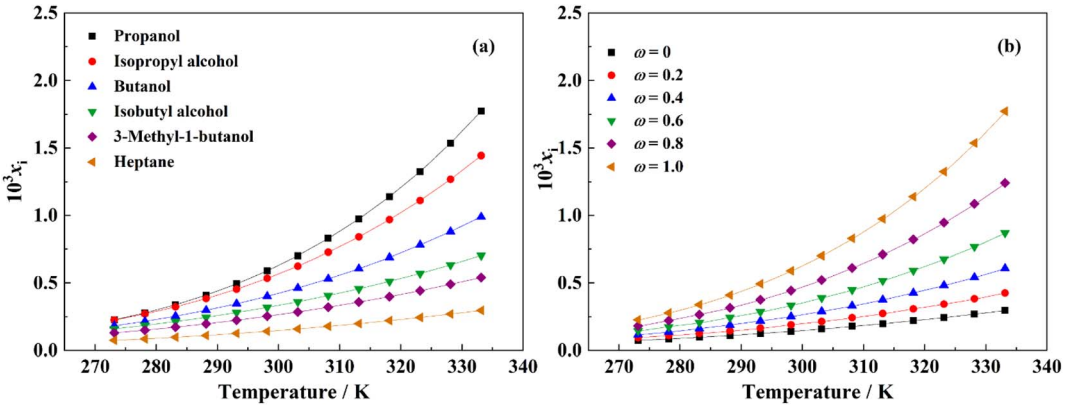

Fig. 6 The experimental (points) and correlated (lines) solubility of form A in pure solvents (a) and propanol + heptane (b), respectively.

The solubility data of form A in various mono-solvents from 273.15 to 333.15 K are collected in Table 2. The solubility data of form A in binary mixtures of propanol and heptane are shown in Table 3. The correlation results by the modified Apelblat equation for the experimental solubility of form A in pure solvents and those in propanol + heptane by the J–A–V model are presented in Fig. 6. The results demonstrate that the solubility of form A show an upward trend as temperature increases throughout all experimental measurements, indicating that this is an endothermic process.

In mono-solvents, the solubility of resmetirom (form A) in alcohols is greater than in alkanes, meanwhile, the solubility of form A in the binary mixed solvent decreases with increasing proportion of heptane, indicating that heptane can be used as an anti-solvent for resmetirom crystal preparation. Obviously, the solubility of form A in various solvents is ranked as: propanol > isopropyl alcohol > butanol > isobutyl alcohol > 3-methyl-1-butanol > heptane.

Model evaluation

Solid–liquid equilibrium is the foundation of separation processes and a prerequisite for chemical production. Drawing from thermodynamic theory, solid–liquid models are established by correlating model parameters with temperature based on experimental solubility. The modified Apelblat equation, λh equation and Wilson model are employed to analyze the correlation of the solubility data of resmetirom (form A) in pure solvents, and J–A–V model are utilized for correlation of solubility data of form A in propanol + heptane, as outlined in Table 4.[33,34] The applicability as well as the accuracy of these four equations for determining the solubility of resmetirom are assessed using the average relative deviation (ARD%) as shown below:[35]

$$\mathrm{ARD\%} = \frac{1}{N}\sum_{i=1}^{N}\left|\frac{x_i^{\mathrm{exp}} - x_i^{\mathrm{cal}}}{x_i^{\mathrm{exp}}}\right| \times 100\% \quad (5)$$

where, x_i^{exp} and x_i^{cal} refer to the experimental and calculated solubility data of resmetirom (form A), respectively. N is the number of data.

The results indicate that the predicted solubility from the equations were in excellent conformity with the measured data. Based on the values of ARD% in Tables S1–S4,† the modified Apelblat equation in mono-solvent exhibits the optimal regression performance for the chosen system, while the Wilson model shows large deviations which is not suitable for this

Table 4 Details of the thermodynamic equations used in this work

Model	Equations	Parameters
Modified Apelblat equation	$\ln(x_i) = A + \frac{B}{T} + C\ln T$	A, B, C
λh equation	$\ln\left(1 + \lambda\frac{1-x_i}{x_i}\right) = \lambda h\left(\frac{1}{T} - \frac{1}{T_m}\right)$	λ, h
	$-\ln(x_i) = \frac{\Delta H}{R}\left(\frac{1}{T} - \frac{1}{T_t}\right) + \ln(\gamma)$	
Wilson model	$\ln(\gamma) = -\ln(x_i + \Lambda_{12}x_2) + x_2\left(\frac{\Lambda_{12}}{x_i + \Lambda_{12}x_2} - \frac{\Lambda_{21}}{x_2 + \Lambda_{21}x_i}\right)$	δ_{12}, δ_{21}
	$\Lambda_{12} = \frac{v_2}{v_1}\exp\left(-\frac{\delta_{12}}{RT}\right)$	
	$\Lambda_{21} = \frac{v_1}{v_2}\exp\left(-\frac{\delta_{21}}{RT}\right)$	
J–A–V model	$\ln x_i = \omega_1\left(A_1 + \frac{B_1}{T}\right) + \omega_2\left(A_2 + \frac{B_2}{T}\right) + \frac{\omega_1\omega_2}{T}\sum_{i=0}^{2}(\omega_1 - \omega_2)^i$	A_1, A_2, B_1, B_2, J_i

Table 5 Thermodynamic parameters of resmetirom (form A) in mono-solvents

Solvent	$\Delta_{dis}H^{\circ}$ (kJ mol^{-1})	$\Delta_{dis}G^{\circ}$ (kJ mol^{-1})	$\Delta_{dis}S^{\circ}$ (J mol^{-1} K^{-1})
Propanol	25.931	17.932	26.490
Isopropyl alcohol	23.421	18.209	17.257
Butanol	21.317	18.942	7.865
Isobutyl alcohol	18.648	19.537	−2.944
3-Methyl-1-butanol	17.867	20.110	−7.428
Heptane	17.368	21.540	−13.815

system. For the mixed solvent, the J–A–V model exhibits the optimal regression performance for the chosen system. This means that the modified Apelblat equation can predict the solubility of the selected mono-solvent at higher or lower temperatures, and the J–A–V model can predict the solubility of the selected mixed solvent.[36]

Thermodynamic analysis of dissolution processes

Utilizing experimental solubility data of the solubility of solids in solvents, the apparent thermodynamic properties of form A in mono-solvents and mixed solvents are calculated in terms of energy. This includes the standard dissolution enthalpy change ($\Delta_{dis}H^{\circ}$), standard entropy change ($\Delta_{dis}S^{\circ}$) and Gibbs free energy change ($\Delta_{dis}G^{\circ}$) of resmetirom (form A) dissolved in different solvents, as illustrated in the following eqn (6)–(9):[37]

$$T_{hm} = N \Big/ \sum_{i=1}^{N}(1/T_i) \quad (6)$$

$$\Delta_{dis}H^{\circ} = -kR \quad (7)$$

$$\Delta_{dis}G^{\circ} = -RT_{hm}d \quad (8)$$

$$\Delta_{dis}S^{\circ} = (\Delta_{dis}H^{\circ} - \Delta_{dis}G^{\circ})/T_{hm} \quad (9)$$

here, T_{hm} denote average harmonic temperature, which is calculated as 301.99 K. k and d are the slope and intercept of the $\ln x$ *versus* $1/T_i - 1/T_{hm}$ curve, respectively.

As shown in Tables 5 and 6, within the range of experimental temperatures, $\Delta_{dis}H^{\circ}$ values are positive for both mono-solvent and binary solvent mixtures, indicating that it is an endothermic process. The heat absorption effect during the dissolution process may be due to the fact that the interaction of solute–solvent molecule is weaker than the solvent–solvent. Furthermore, in mono-solvent systems, the $\Delta_{dis}S^{\circ}$ values that describe the randomness of the dissolution behavior are positive in propanol, isopropyl alcohol, and butanol. In the mixed solvent of propanol and heptane, the $\Delta_{dis}S^{\circ}$ values are also positive at $\omega = 0.2$, 0.4 and 0.6, suggesting that the dissolution process is entropy-favored. When the dissolution process occurred of resmetirom molecules, the arrangement of solvent molecules is thrown into disarray, resulting the entropy of system is increasing.[38] At the same time, $\Delta_{dis}G^{\circ}$ values for the dissolution behavior of form A are also positive in all chosen solvent systems. The $\Delta_{dis}G^{\circ}$ during dissolution determines the ease of dissolution, the smaller the $\Delta_{dis}G^{\circ}$ values, the lower the energy barrier to be overcome in the dissolution behavior and the higher the solubility of the solute.[39]

Table 6 Thermodynamic parameters of resmetirom (form A) in mixed solvents

ω	$\Delta_{dis}H^{\circ}$ (kJ mol^{-1})	$\Delta_{dis}G^{\circ}$ (kJ mol^{-1})	$\Delta_{dis}S^{\circ}$ (J mol^{-1} K^{-1})
0.2	24.177	18.644	18.322
0.4	22.531	19.369	10.471
0.6	20.818	20.086	2.425
0.8	18.956	20.813	−6.150

Binding energy analysis based on DFT

According to Hossain, the dissolution of solutes in certain solvents is essentially governed by a two-stage process.[40] Firstly, a relatively large pore or cavity is generated in the solvent phase to accommodate the solute molecule, and then the solute molecule enters the pore and interacts with the surrounding solvent molecules. Based on above, the solubility of a solute is closely related not only to the properties of the chosen solvent but also to the solute–solvent interactions. Therefore, DFT simulations were used to calculate the interaction forces and ΔE between form A and the selected solvents.

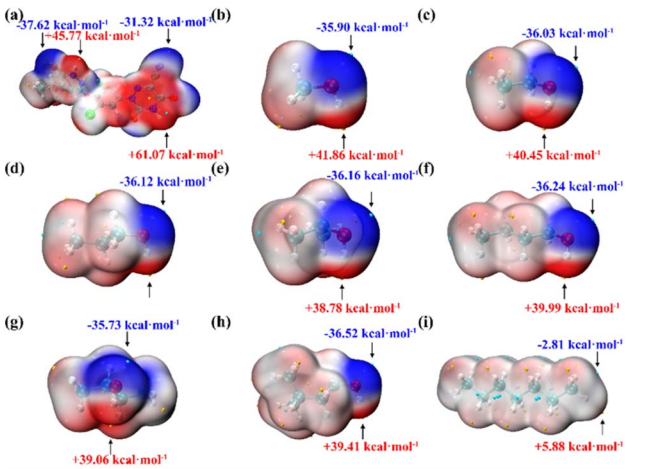

Fig. 7 MEPs of resmetirom (a), methanol (b), ethanol (c), propanol (d), isopropyl alcohol (e), butanol (f), isobutyl alcohol (g), 3-methyl-1-butanol (h), heptane (i).

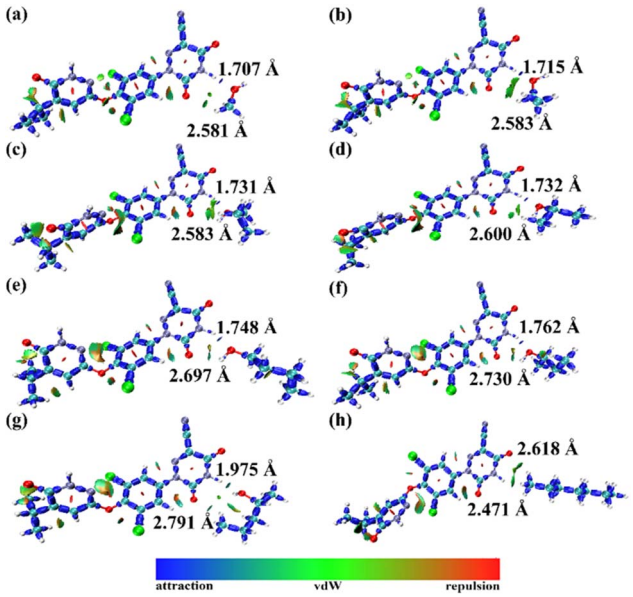

Fig. 8 Isosurface diagrams of IRI analysis of solute with methanol (a), ethanol (b), propanol (c), isopropyl alcohol (d), butanol (e), isobutyl alcohol (f), 3-methyl-1-butanol (g) and heptane (h).

MEPs are based on the attraction between positive and negative potentials, which reveals the possible binding sites between solute and solvent molecules and facilitates the generation of initial configuration. The MEPs of resmetirom and various solvent molecules are depicted in Fig. 7. Blue zone is positive potential and red zone is negative potential. Furthermore, the yellow and cyan balls correspond to the points of maximum and minimum electrostatic potentials, respectively. The magnitude of the electrostatic potential values reveals that the H atom in the R3 ring of the resmetirom molecule corresponds to the extreme value of the surface electrostatic potential (61.07 kcal mol^{-1}), while in the solvent molecules of alcohols, the O atom on the hydroxyl group corresponds to the extreme value of the surface electrostatic potential. Above sites are predicted as bonding sites between resmetirom and solvent molecules for subsequent configuration.

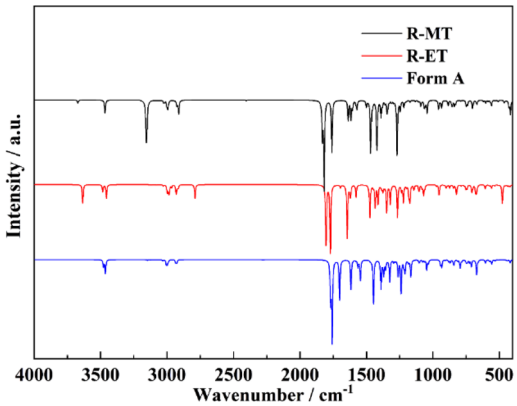

Fig. 9 The theoretical spectra of form A, R-MT and R-ET.

The optimized schematic of IRI resmetirom–solvent unit is shown in Fig. 8. The isosurface diagrams exhibit two isosurface domains of hydrogen bonds (blue) as well as van der Waals force (green), respectively. The main physicochemical properties and related calculated energy of the selected solvents are shown in Table 7, indicate that the solubility decreases with decreasing solvent polarity. Hydrogen bond acceptor and donor capabilities are both presented in alcohol solvents, while the R3 ring of resmetirom also contains an O atom and an H atom, so two hydrogen bonds will appear in unit, represented by the blue isosurface area. However, due to the difference in solvent polarity, the interaction force is varied, and the magnitude of the energy can be judged from the marked-out distance and the color of the isosurface. For example, the distances between the hydrogen bonds are the shortest in the unit of resmetirom + methanol, at 1.707 Å and 2.581 Å, respectively. While hydrogen bond acceptor and donor are lacked in the molecular structure of heptane, a large number of green isosurface area is performed, indicating there is only dispersion force rather than hydrogen-bond interaction. Therefore, it can be concluded that hydrogen bonds play primary roles in the dissolution of resmetirom in the studied solvents.

The ΔE between resmetirom (form A) and solvents are collected in Table 7. Specifically, the ΔE of these solvent–solute is as follows: methanol (−17.25) > ethanol (−9.75) > propanol

Table 7 Main physicochemical properties of the solvents and ΔE between the corresponding units

Solvent	π^a	$\sum\alpha^b$	$\sum\beta^c$	$E_A + E_B{}^d$	$E_{unit}{}^e$	ΔE^f (kcal mol^{-1})
Methanol	0.60	0.43	0.47	−2436.351	−2436.378	−17.25
Ethanol	0.54	0.37	0.48	−2359.950	−2359.966	−9.75
Propanol	0.48	0.37	0.48	−2399.271	−2399.286	−9.02
Isopropyl alcohol	0.48	0.33	0.56	−2399.279	−2399.293	−8.92
Butanol	0.47	0.37	0.48	−2438.600	−2438.614	−8.83
Isobutyl alcohol	0.40	0.37	0.48	−2438.594	−2438.606	−7.87
3-Methyl-1-butanol	0.40	0.37	0.48	−2477.915	−2477.927	−7.48
Heptane	−0.08	0.00	0.00	−2481.346	−2481.353	−4.07

[a] The polarity and dipole moment of solvent.[41] [b] Hydrogen bond donor ability.[42] [c] Hydrogen bond acceptor ability.[42] [d] Energy of two monomers in their respective basis sets. [e] Total energy after correction. [f] Binding energy between two molecules.

(−9.02) > isopropyl alcohol (−8.92) > butanol (−8.83) > isoamyl alcohol (−7.87) > 3-methyl-1-butanol (−7.48) > heptane (−4.07). The ΔE between solute and solvent is always decreased accompanied by an increase in c-chain length, and the lower value of ΔE, the higher the solubility, which is consistent with the experimental results.

Validation of quantitative analysis methods

The standard curve is established by FTIR to quantitatively analyze the polymorphic composition of resmetirom during the transformation from form A to solvates, and the kinetics is also studied. Since the dynamic view of the calculated vibration frequencies are allowed to be viewed through the Gaussian View 6.0 software, and the peaks that reflected the interaction force between resmetirom and solvents are chosen and used in a quantitative model. The infrared spectra of R-ET and R-MT are very similar and therefore the same bands can be selected for analysis. In Fig. 9, the comparison of theoretical spectra of three solids are compared. In addition, the selected ranges and relevant vibrations are shown in Table 8.

In Fig. 10, the actual and predicted concentration of solvents in the binary mixture based on PLSR are compared. The model correlation coefficients are obtained from the quantitative analysis using the full spectral bands when the solvent compound is in the 0–100% concentration range depicted in Fig. 10(a). In addition, the accuracy of the model is improved significantly with the model correlation coefficient rising to 0.999 by combining with the specific bands selected by DFT and PLSR, as shown in Fig. 10(b). The results suggest that the combination of variable selection and DFT calculations is feasible for the analysis of solvent compound concentration in the complex range.

Process of solid transformation

Based on the high-precision quantitative analysis method, the solid transformation of form A in methanol and ethanol has been studied from 303.15 to 323.15 K with the same suspension density as well as stirring. The solid transformation of form A to its solvates is graphically shown in Fig. 11. Generally, the transformation rate from the form A to the solvates decreases with increasing temperature, which is probably because the supersaturation of solvates (*i.e.* the difference between the concentration of solvates and their solubility) at lower temperature is larger than that at higher temperature, and the larger supersaturation of solvates is benefit for the formation of solvate nuclei.[43] Based on the rate of transition in Fig. 11, it can be seen that three stages of solid transformation. Initially, the number of nuclei formed by crystallization is small and therefore the crystallization rate is relatively slow. As the number of nuclei in the solution increases, the crystallization rate gradually increases, driven by the degree of supersaturation. Finally, as the crystals precipitate, resulting in a decrease in the crystallization rate after reaching its maximum value. That is, the transformation process is driven by the solubility difference between form A and solvates.[44] Besides, it is obvious that the transformation time of form A to R-MT is faster than that of form A to R-ET, which is probably because the binding capacity between resmetirom and methanol is stronger than that between resmetirom and ethanol.

Table 8 Variable selection range and corresponding relative vibration mode

Spectral range (cm^{-1})	Related vibrations
3720–3180	The stretching vibration of N–H in amide and the O–H stretching vibrations in hydroxyl of intermolecular hydrogen bonding
1800–1600	The N–H in-plane bending vibration in R1 ring; the stretching vibration of carbonyl group in amide
1275–1150	The N–H in-plane bending vibration caused by the C–N and N–N stretching vibration of R1 ring
980–850	The in-plane bending vibration of N–H of R1 ring; the out-of-plane rocking vibration of N–H of R3 ring
645–600	The out-of-plane rocking vibration of N–H of R1 ring

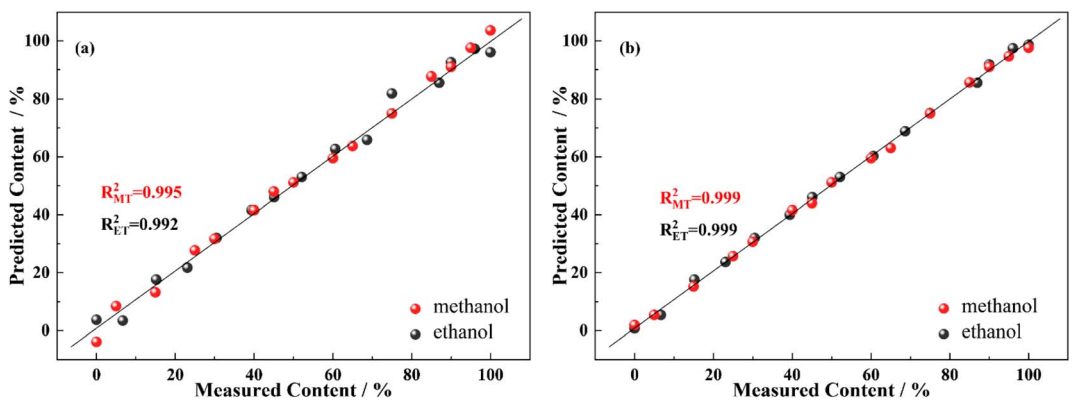

Fig. 10 The standard curves for quantitative analysis with a full spectrum (a) and with selected specific bands (b), respectively.

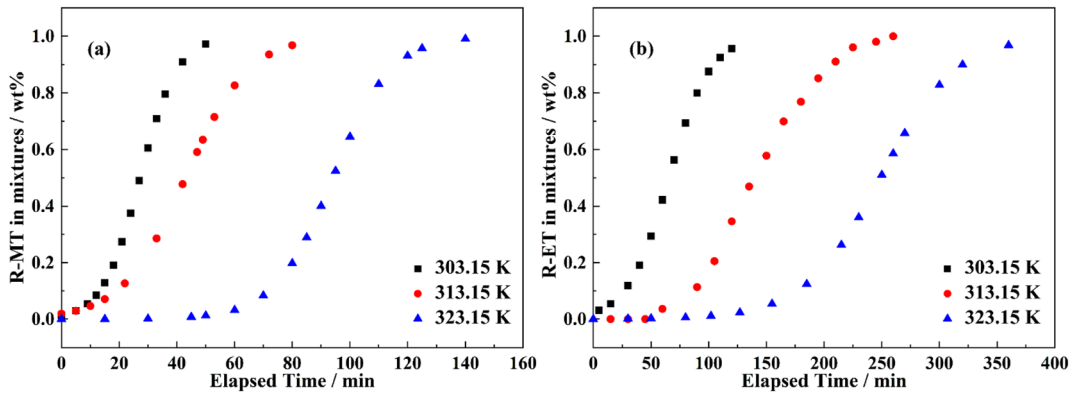

Fig. 11 Transformation profiles at different temperatures in methanol (a) and ethanol (b).

Table 9 Details of the kinetic equations and the correlation coefficient of the models for resmetirom (form A) to solvate

Model name	Equation	Parameters
M1: Prout–Tompkins	$\ln\left[\frac{\alpha}{(1-\alpha)}\right] = kt + c$	k, c
M2: Avrami–Erofeev ($n = 3$)	$[-\ln(1-\alpha)]^{\frac{1}{3}} = kt$	
M3: first order	$-\ln(1-\alpha) = kt$	
M4: two dimensional phase boundary	$1-(1-\alpha)^{\frac{1}{2}} = kt$	
M5: three dimensional phase boundary	$1-(1-\alpha)^{\frac{1}{3}} = kt$	
M6: 1D diffusion	$\alpha^2 = kt$	
M7: 2D diffusion	$(1-\alpha)\ln(1-\alpha) + \alpha = kt$	
M8: 3D diffusion-Jander equation	$\left[1-(1-\alpha)^{\frac{1}{3}}\right]^2 = kt$	
M9: 3D diffusion-Ginstling–Brounshtein equation	$\left(1-\frac{2\alpha}{3}\right)-(1-\alpha)^{\frac{2}{3}} = kt$	

Solid–solid transformation models are theoretical and mathematical description of experiment results, which are usually based on mechanical assumptions or experience. The goal of kinetic research is always to acquire rate constants k, which can be utilized for characterizing the reaction mechanism.[45] Similarly, the study of transformation processes involves the same objective. Various solid–solid kinetics models are employed to evaluate the time-dependent functions of the solid transformation rate at different temperatures. And α represents the content of the predicted solid transformation with FTIR spectra, k denotes the reaction rate constant, t stands for the solid transformation time. Nine classic solid–solid kinetics models are used to verify the process from form A to solvates, and the kinetic equation and relevant coefficients are shown in Table 9.[46–48]

Table 10 Correlation coefficient (R^2) of the model of resmetirom (form A) to solvates

	Methanol			Ethanol		
	308.15 K	318.15 K	328.15 K	308.15 K	318.15 K	328.15 K
M1	0.997	0.999	0.998	0.996	0.998	0.998
M2	0.912	0.982	0.907	0.984	0.998	0.991
M3	0.995	0.995	0.992	0.989	0.997	0.997
M4	0.922	0.936	0.999	0.987	0.938	0.984
M5	0.925	0.993	0.995	0.990	0.962	0.978
M5	0.913	0.917	0.984	0.972	0.982	0.982
M7	0.980	0.982	0.977	0.978	0.960	0.968
M8	0.907	0.960	0.957	0.873	0.961	0.950
M9	0.956	0.982	0.988	0.967	0.989	0.989

Based on the equations and correlation coefficients in Table 10, optimal results for the transformation of form A to R-MT and R-ET at different temperatures are obtained from M1. M1 is a self-catalytic model in which the solvate plays a catalytic role along with production. To determine the activation energy, k is always assumed follows the Arrhenius equation:[49]

$$\ln k = -\frac{E_a}{RT} + \ln A \quad (10)$$

where E_a and A represent the activation energy and the pre-exponential factor of the process, respectively. Regression analysis is based on the eqn (10) to calculate the activation energy of the solid transformation of form A in methanol (E_a =

−17.79 kJ mol^{-1}) and ethanol (E_a = −15.24 kJ mol^{-1}), respectively.

Conclusions

The solubility of resmetirom (form A) in various solvents is ranked as: propanol > isopropanol > butanol > isobutyl alcohol > 3-methyl-1-butanol > heptane, in which propanol and heptane can be chosen as the good and the poor solvent for its anti-solvent crystallization, respectively. The modified Apelblat equation and the J–A–V model achieve the highest correlation accuracy for the experimental solubility data in mono-solvents and heptane + propanol, respectively. DFT calculation and solvent parameters analyses indicate that hydrogen-bonding plays primary roles in the dissolution process of resmetirom (form A) in the studied solvents. Furthermore, a high-precision quantitative method for probing transformation process is firstly and successfully established. Using this efficient and convenient approach, it is found that the rate of transformation from form A to methanol solvate or ethanol solvate is decreased with increasing temperature from 303.15 to 323.15 K, with activation energies of −17.79 and −15.24 kJ mol^{-1}, respectively. In sum, this work shall definitely afford necessary solubility data and solvent selection for the design of the crystallization process of resmetirom (form A) in industry.

Author contributions

Chang Liu: data collection, writing original draft. Yue Xu: data analysis. Haikuan Yuan: supervision, validation. Guangxin Tian: methodology. Xiaolan Qin: editing. Boxuan Lou: validation. Xijian Liu: reviewing. Lijuan Zhang: conceptualization. Jie Lu: supervision, resources.

Conflicts of interest

The authors declared that they have no conflicts of interest to this work.

Acknowledgements

We appreciated the National Natural Science Foundation of China (No. 21978165, 92156020, 22081340412 and 22078191) to support this work.

Notes and references

1 D. Singhal and W. Curatolo, *Adv. Drug Delivery Rev.*, 2004, **56**, 335–347.
2 K. M. Lutker, R. Quiñones, J. Xu, A. Ramamoorthy and A. J. Matzger, *J. Pharm. Sci.*, 2011, **100**, 949–963.
3 P. Klitou, C. M. Pask, L. Onoufriadi, I. Rosbottom and E. Simone, *Cryst. Growth Des.*, 2020, **20**, 6573–6584.
4 D. Braun and U. Griesser, *CrystEngComm*, 2017, **19**, 3566–3572.
5 R. Chang, Q. Fu, P. Yu, L. Wang, Y. Li, W. Du, C. Chang and A. Zeng, *RSC Adv.*, 2016, **6**, 85063–85073.
6 X. Xiong, Q. Du, X. Zeng, J. He, H. Yang and H. Li, *RSC Adv.*, 2017, **7**, 23279–23286.
7 G. Wang, Y. Ma, Y. Wang, H. Hao and Y. Jiang, *Org. Process Res. Dev.*, 2015, **19**, 1820–1825.
8 V. Suitchmezian, I. Jeß and C. Näther, *J. Pharm. Sci.*, 2008, **97**, 4516–4527.
9 Y.-H. Yun, Y.-Z. Liang, G.-X. Xie, H.-D. Li, D.-S. Cao and Q.-S. Xu, *Analyst*, 2013, **138**, 6412–6421.
10 J. Zhang, H. Yan, Y. Xiong, Q. Li and S. Min, *RSC Adv.*, 2019, **9**, 6708–6716.
11 J. Ludwig, *Mayo Clin. Proc.*, 1980, **55**, 434–438.
12 F. Schaffner and H. Thaler, *Prog. Liver Dis.*, 1986, **8**, 283.
13 Z. M. Younossi, A. B. Koenig, D. Abdelatif, Y. Fazel, L. Henry and M. Wymer, *Hepatology*, 2016, **64**, 73–84.
14 A. Kannt, P. Wohlfart, A. N. Madsen, S. S. Veidal, M. Feigh and D. Schmoll, *Br. J. Pharmacol.*, 2021, **178**, 2412–2423.
15 S. Harrison, A. Mangia, P. Lasierra-Resa, M. S. Cubberley, R. Taub, G. Neff, N. Alkhouri and M. Bashir, *Dig. Liver Dis.*, 2022, **54**, S48.
16 G. X. Tian, Y. Luo, B. X. Lou, J. Sui, X. Qin, Y. Shen, X. Zhu and J. Lu, *J. Mol. Liq.*, 2023, **369**, 120857.
17 P. Manjusha, S. Muthu and B. Raajaraman, *J. Mol. Struct.*, 2020, **1203**, 127394.
18 F. Jacinto, L. Siqueira and W. A. Alves, *J. Raman Spectrosc.*, 2010, **40**, 1585–1590.
19 R. Xu, B. Hou, N. Wang, Y. Lou, Y. Li, J. Huang and H. Hao, *J. Mol. Liq.*, 2018, **252**, 194–202.
20 S. Liu, E. G. Macaringue, X. Li, L. Jia, Y. Liu and J. Gong, *J. Mol. Liq.*, 2017, **238**, 411–422.
21 Y. Cheng, D. Wang, Z. Zhang and Z. Wang, *RSC Adv.*, 2015, **5**, 80548–80552.
22 V. Consonni, G. Baccolo, F. Gosetti, R. Todeschini and D. Ballabio, *Chemom. Intell. Lab. Syst.*, 2021, **213**, 104313.
23 S. Karimi, J. Feizy, F. Mehrjo and M. Farrokhnia, *RSC Adv.*, 2016, **6**, 23085–23093.
24 T. Topal, Y. Zorlu and N. Karapınar, *J. Mol. Struct.*, 2021, **1239**, 130514.
25 T. Lu and F. Chen, *J. Comput. Chem.*, 2012, **33**, 580–592.
26 T. Lu and Q. Chen, *Chem.: Methods*, 2021, **1**, 231–239.
27 L. Bondesson, E. Rudberg, Y. Luo and P. Sałek, *J. Comput. Chem.*, 2008, **29**, 1725–1732.
28 Z. Ren, Y. Zeng, Y. Hua, Y. Cheng and Z. Guo, *J. Chem. Eng. Data*, 2014, **59**, 2517–2522.
29 M. Singh, *J. Cryst. Growth*, 2014, **396**, 14–23.
30 R. Van Santen, *J. Phys. Chem.*, 1984, **88**, 5768–5769.
31 Z. Fang, L. Zhang, S. Mao, S. Rohani, J. Ulrich and J. Lu, *J. Chem. Thermodyn.*, 2015, **90**, 71–78.
32 M. Mirmehrabi, S. Rohani, K. Murthy and B. Radatus, *Int. J. Pharm.*, 2004, **282**, 73–85.
33 L. Huang, X. Li, R. Han, Y. Li, L. Xu, Z. Zeng and K. Wu, *J. Mol. Liq.*, 2022, **363**, 119847.
34 M. Xue, D.-z. Huang, K.-x. Yang, L.-z. Chen, Z.-h. Zheng, Y. Xiang, Q.-w. Huang and J.-l. Wang, *J. Mol. Liq.*, 2021, **330**, 115639.
35 S. N. Mirheydari, M. Barzegar-Jalali, F. Martinez and A. Jouyban, *Phys. Chem. Liq.*, 2020, **58**, 769–781.
36 A. Jouyban, *Pharmazie*, 2007, **62**, 365–367.

37 C. Zhang, A. Jouyban, H. Zhao, A. Farajtabar and W. E. Acree Jr, *J. Mol. Liq.*, 2021, **326**, 115219.
38 H. Zhang, Y. Yang, M. Zhu, S. Jiang, S. Xu, S. Du, B. Yu and J. Gong, *J. Mol. Liq.*, 2017, **240**, 162–171.
39 C. Li, H. Wang, W. Huang, T. Wen, J. Xu, J. Ouyang and C. Zhang, *J. Mol. Liq.*, 2021, **339**, 116733.
40 S. Hossain, A. Kabedev, A. Parrow, C. A. Bergström and P. Larsson, *Eur. J. Pharm. Biopharm.*, 2019, **137**, 46–55.
41 C.-H. Gu, H. Li, R. B. Gandhi and K. Raghavan, *Int. J. Pharm.*, 2004, **283**, 117–125.
42 M. H. Abraham, *Chem. Soc. Rev.*, 1993, **22**, 73–83.
43 L. Jia, Q. Yin, L. Zhou, X. Zhang, C. Wang, W. Du and L. Zhou, *RSC Adv.*, 2018, **8**, 9697–9706.
44 F. Tian, H. Qu, A. Zimmermann, T. Munk, A. C. Jørgensen and J. Rantanen, *J. Pharm. Pharmacol.*, 2010, **62**, 1534–1546.
45 A. Khawam and D. R. Flanagan, *J. Phys. Chem. B*, 2006, **110**, 17315–17328.
46 L. Zhou, Q. Yin, S. Du, H. Hao, Y. Li, M. Liu and B. Hou, *RSC Adv.*, 2016, **6**, 51037–51045.
47 T. Liu, Y. Ran, B. Wang, W. Dong, W. U. Songgu and J. Gong, *Front. Chem. Sci. Eng.*, 2014, **8**, 55–63.
48 K. A. Alkhamis, M. S. Salem and R. M. Obaidat, *J. Pharm. Sci.*, 2006, **95**, 859–870.
49 L. E. O'Brien, P. Timmins, A. C. Williams and P. York, *J. Pharm. Biomed. Anal.*, 2004, **36**, 335–340.